Evaluation of the microlayer contribution to bubble growth in horizontal pool boiling with a mechanistic model that considers dynamic contact angle and base expansion

Ding, W.; Krepper, E.; Hampel, U.;

Originally published:

June 2018

International Journal of Heat and Fluid Flow 72(2018), 274-287

DOI: https://doi.org/10.1016/j.ijheatfluidflow.2018.06.009

Perma-Link to Publication Repository of HZDR:

https://www.hzdr.de/publications/Publ-27665

Evaluation of the microlayer contribution to bubble growth in horizontal pool boiling with a mechanistic model that considers dynamic contact angle and base expansion

Wei Ding[1], Eckhard Krepper[1], Uwe Hampel[1,2]*

[1] Institute of Fluid Dynamics, Helmholtz-Zentrum Dresden-Rossendorf, Dresden, Germany

[2] AREVA Endowed Chair of Imaging Techniques in Energy and Process Engineering, Technische Universität Dresden, Germany

Abstract

Recently a new mechanistic model for pool and nucleate flow boiling was developed in our group. This model is based on the balance of forces acting on a bubble and considers the evaporation of the microlayer underneath the bubble, thermal diffusion around the cap of bubble due to the super-heated liquid and condensation due to the sub-cooled liquid. Compared to other models we particularly consider the temporal evolution of the microlayer underneath the bubble during the bubble growth by consideration of the dynamic contact angle and the dynamic bubble base expansion. This enhances, in our opinion, the model accuracy and generality. In this paper we further evaluate this model with experiments and direct numerical simulation (DNS) in order to prove the importance of dynamic contact angle and bubble base expansion.

Keywords: nucleate boiling; microlayer; force balance; dynamic contact angle; dynamic base expansion; bubble geometry

1. Introduction

Nucleate boiling is an efficient heat transfer process. Its physical modelling is still not fully mature as it involves complex two-phase fluid dynamics with mass, momentum and energy transfer at the liquid-vapor interface and further heat conduction through solid walls. The bubble dynamics of nucleation boiling has been heavily investigated since the 1950s, first in pool boiling. In the 1950s Forster and Zuber [1] as well as Plesset and Zwick [2] modelled the bubble growth in a uniformly superheated liquid. Zuber [3] extended this model to non-uniform temperature fields. Then Mikic et al. [4], Prosperetti and Plesset [5], and Labuntsov [6], derived dimensionless relations for inertia controlled and heat (or thermal diffusion) controlled growth. Cooper and Loyd [7] identified a thin liquid microlayer underneath the bubbles and modelled it on the basis of experimental findings. Then Van Stralen et al. [8] proposed a model based on the evaporation of the microlayer underneath the bubble and heat diffusion from a relaxation microlayer around the bubble. In 1993, Klausner et al. [9] developed a model based on the balance of the forces acting on the bubble to predict its departure and lift-off. The authors obtained satisfactory prediction accuracy against their own data of flow boiling with refrigerant R113. They recommended a fixed bubble base diameter (contact diameter) of 0.09 mm, an advancing contact angle of $\pi/4$ and a receding contact angle of $\pi/5$. Later, modified versions of the Klausner model have been brought up by others with other values of base diameter, advancing and receding contact angle to predict their own experimental data. Examples are Yun et al. [10], Situ et al. [11], Sugrue [12], Thorncroft et al. [13] and Chen [14]. Klausner applied the Mikic model to simulate the bubble growth while Situ and most of the latter authors employed the Zuber [4] formulation. Zuber included in his formulation a parameter b to account for bubble sphericity. This parameter has been used by the latter authors with different values between 0.24 and 24 to fit the models with their experimental data [15]. Yun et al. [10] improved Klausner's model by incorporating a bubble condensation model as well as evaluating the model for a wider range of pressure, temperature, and flow rates for water. More recently, in 2015, Colombo and Fairweather [15] developed a mechanistic

model to simulate the bubble growth and departure. In the model, they considered the contribution of the microlayer, the superheated thermal liquid layer and the condensation to bubble growth (Figure 1). Based on the suggested contact angles from Klausner et al. [9] and other empirically measured contact angles, the model gave a good agreement with data from different experiments. Later in 2017, Raj et al. [16] tried to formulate a similar model as an analytical solution with countable validations. In 2018, Mozzocco et al. [17] developed a model for the mechanistic prediction of bubble departure and lift off. Different to the models of Colombo and Fairweather [15] and Raj et al. [16], where the condensation is being modelled with the correlation of Ranz and Marshall [22], the author applied a parametric constant to capture the effect of convective heat transfer for saturated and subcooled flow conditions. The model was also validated with different experimental data. It was found that the bubble dynamics models still require some empirical constants under different conditions. For the force analysis in the models, the bubble is always considered as a hemisphere or truncated sphere and the impact of bubble deformation during the bubble growth is not considered.

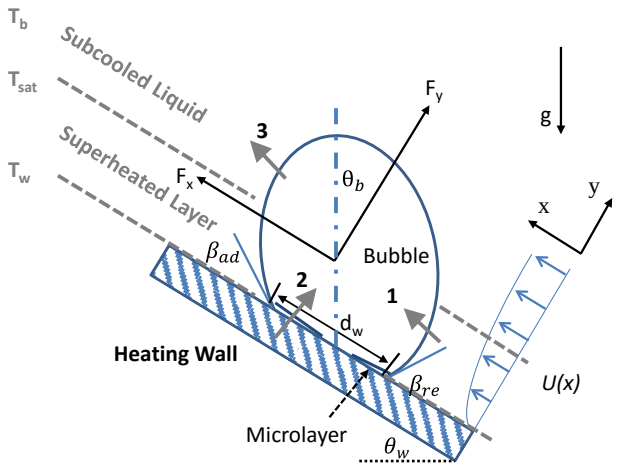

Figure 1: Schematic sketch of the bubble during its growth: β_{ad} and β_{re} are the advancing and receding side contact angles, d_w is the bubble base diameter and θ_w is wall orientation angle, (1) evaporation from superheated layer, (2) evaporation from microlayer, (3) condensation.

Basing on previous studies, e.g. of Colombo and Fairweather [15], Raj et al. [16] and Mozzocco et al. [17], our group recently developed a mechanistic model to simulate and predict the bubble departure in pool boiling and flow boiling on a smooth wall. The model considers the heat transfer contributions from the microlayer, the superheated layer surrounding the bubble and condensation at the bubble's top. Moreover, the formation, evaporation and depletion of the microlayer (dryout formation) as well as the change of the bubble geometry during the bubble growth are considered in this model. In our opinion, this enhances the model accuracy and generality. The calculation of the microlayer is supported by the consideration of dynamic contact angle and bubble base expansion. The differences between the present model and previous models are given in Table 1.

In this work, our model of horizontal pool boiling will be applied to evaluate the role of the microlayer beneath the bubble to the bubble growth. We compare results obtained with our new model with the experiments from Duan et al. [19] for pool boiling of water at 1 atm and corresponding Direct Numerical Simulations (DNS) from Sato and Niceno [20]. The comparisons help to verify the concept related to the consideration of dynamic contact angle, dynamic base expansion and geometry change with bottleneck.

Table 1: Published models for calculating bubble growth and departure ("●" indicates that the respective physical mechanism is modelled)

Authors	Growth model			Departure model (force balance model)		
	Microlayer	Superheated thermal layer	Condensation	Force balance	Contact angle/ base expansion	Geometry change
Zuber [3]		●				
Plesset and Zwick [2]		●				
Mikic et al. [4]		●				
Cooper and Lloyd [7]	●					
Van Stralen et al. [8]	●	●				
Klausner et al. [19]		●		●	● Constant/ Constant	
Yun et al. [10]		●	●	●	● Constant/ $d_w = 2r_b/15$	
Colombo and Fairweather [15]	● (no dryout)	●	●	●	● Constant and case dependent/ constant	
Raj et al. [16]	● (no dryout)	●	●	●	● No statement	
Mazzoco et al. [17]	● (no dryout)	●	●	●	● No statement	
Present study	● (incl. formation, evaporation and depletion (dryout))	●	●	●	● Dynamic /Dynamic	●

2. Bubble Growth and Detachment Model

2.1 Bubble Growth Rate

The bubble growth process can be divided into two periods: the inertia controlled period and the thermal diffusion controlled period [4]. When the bubble is still small, its growth in diameter is quite fast and determined by the inertia of the liquid being displaced. Hence this period is referred to as inertia controlled growth. In this period a microlayer is formed underneath the bubble, which was postulated and proven by Cooper in 1969 [7]. After a while the growth of the bubble diameter becomes slower and it is no longer limited by liquid displacement but by evaporative heat flux at the gas-liquid interface. This is hence referred to as thermal diffusion controlled growth. An essential evaporative heat flux contribution in this period comes from the microlayer, which is well superheated. In this period, the microlayer underneath the bubble extends with the growth of the bubble (Figure 2). When the bubble grows into the sub-cooled liquid, where the temperature is lower than saturation temperature, the condensation slows down the growth of bubble and sometimes even shrinks the bubble.

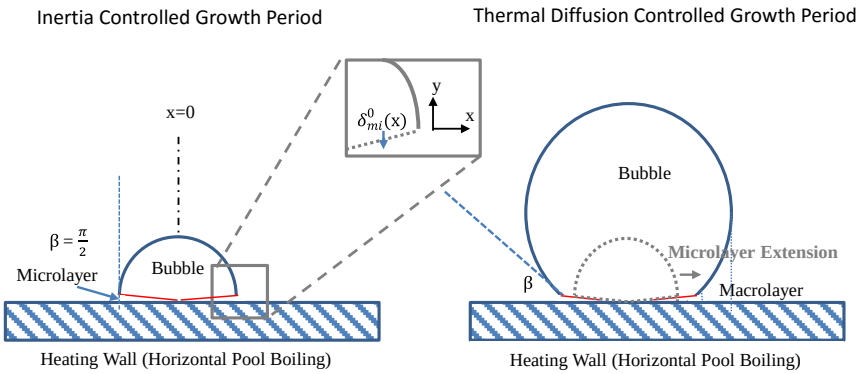

Figure 2: Schematic sketch of the inertia and thermal diffusion controlled bubble growth on a horizontal heating surface.

Mikic et al. [4] derived a model for the inertia controlled growth of a bubble on a heated surface. Their analysis, which bases on the Clausius-Clapeyron equation, relates the time dependent bubble radius

$$r_b(\mathrm{t}) = \left\{\frac{\pi}{7}\left(\frac{T_\mathrm{W}-T_{sat}}{T_{sat}}\right)\frac{h_{fg}\rho_g}{\rho_l}\right\}^{1/2} t, \tag{1}$$

to the wall temperature T_W and the saturation temperature of the liquid T_{sat} given the latent heat h_{fg} and the densities of gas and liquid ρ_g, ρ_l. Mikic et al. further introduced the constants

$$A = \sqrt{\frac{\pi}{7}\left(\frac{T_\mathrm{W}-T_{sat}}{T_{sat}}\right)\frac{h_{fg}\rho_g}{\rho_l}} \quad and \quad B = Ja\sqrt{\frac{12\alpha_l}{\pi}}, \tag{2}$$

with the Jacob number $Ja = \frac{\rho_l c_{pl}(T_w-T_{sat})}{\rho_g h_{fg}}$, the thermal diffusivity α_l and the heat capacity c_{pl} of the liquid and claimed that for $\frac{A^2 t}{B^2} \ll 1$ growth is inertia controlled while for $\frac{A^2 t}{B^2} \gg 1$ it is thermal diffusion controlled. As in an applicable model we need to have a clear distinction, we will further consider $\frac{A^2 t}{B^2} = 1$ as a demarcation value between the two states. With that, the maximal inertia controlled bubble radius is given as

$$r_{m,g} = \frac{B^2}{A}. \tag{3}$$

In the inertia controlled growth period the shape of the bubble is hemispherical. The heat flux is given by heat conduction through the microlayer on the superheated surface

$$\dot{Q} = k_l \frac{(T_w - T_{sat})}{\delta^0_{mi}(x)} = k_l \frac{\Delta T_{sat}}{\delta^0_{mi}(x)}, \quad (4)$$

where k_l is liquid thermal conductivity, $\delta^0_{mi}(x)$ the initial microlayer thickness at a distance x from the nucleation site (Figure 2) and ΔT_{sat} the wall superheat. According to our assumption that $\frac{A^2 t}{B^2} = 1$ demarcates the transition, the thermal diffusion controlled growth period sets in when the bubble reaches the maximal inertia controlled bubble radius $r_{m,g}$. Then bubble growth is mainly fed by the evaporation of the microlayer and the superheated liquid surrounding the bubble cap. Considering the heat balance between the latent heat of the liquid microlayer evaporation and the heat conducted through the microlayer we find for the microlayer thickness $\delta_{mi}(t,x)$ that

$$-\rho_l h_{fg} \frac{d\delta_{mi}(t,r)}{dt} = \frac{k_l \Delta T_{sat}}{\delta_{mi}(t,x)}. \quad (5)$$

Considering further the mass balance the volumetric bubble growth rate $\dot{V}_{mi,g}$ can be calculated from

$$\dot{V}_{mi,g} = \dot{V}_{mi,l} \frac{\rho_l}{\rho_g} = \frac{\rho_l}{\rho_g} \pi \int_0^{r_w} \frac{d\delta_{mi}(t,x)}{dt} x dx, \quad (6)$$

where $\dot{V}_{mi,l}$ is the evaporated liquid volume rate from the microlayer and r_w is the bubble base radius. In the thermal diffusion controlled period the shape of the bubble changes from hemispherical to truncate regular spherical and a liquid layer is formed underneath the bubble outside of the microlayer which is termed macrolayer [21] (Figure 2).

The thermal diffusion controlled growth, sometimes referred to as macrolayer evaporation, can be calculated by the Labuntsov solution [6]

$$\left(\frac{dr_b}{dt}\right)_{ma} = \frac{1}{2} B_1 t^{-\frac{1}{2}}, \quad (7)$$

where $B_1 = c_1 Ja \alpha_l{}^{1/2}$ and $c_1 = \left(\frac{12}{\pi}\right)^{1/2} \left[1 + \frac{1}{2}\left(\frac{\pi}{6Ja}\right)^{2/3} + \frac{\pi}{6Ja}\right]^{1/2}$.

The bubble radius growth rate in the thermal diffusion controlled growth period is calculated as

$$\frac{dr_b}{dt} = \frac{\dot{V}_{mi,g}}{A_b} + \left(\frac{dr_b}{dt}\right)_{ma} (1 - f_{sub}), \quad (8)$$

where A_b is the bubble surface area and f_{sub} is the portion of the bubble surface in contact with the sub-cooled liquid. Eventually, condensation, that occurs when the bubble comes in contact with the sub-cooled liquid, is also accounted for in this model. The bubble shrinkage rate is determined by the

heat balance between the latent heat of condensed steam and the condensation heat flux based on the Ranz and Marshall correlation [15, 16, 22]. With Eq. (8) the bubble growth rate can be written as

$$\frac{dr_b}{dt} = \frac{\dot{V}_{mi,g}}{A_b} + \left(\frac{dr_b}{dt}\right)_{ma}(1 - f_{sub}) - \frac{\mathrm{k}_l\left((2+0.6Re^{0.5}\mathrm{Pr}^{0.3})(T_{sat}-T_{sub})\right)}{2r_b\rho_g h_{fg}} f_{sub}. \quad (9)$$

Superheat is required to activate the bubble on the wall. A liquid layer with the temperature between the superheated wall temperature T_{wall} and saturation temperature T_{sat} is considered as a superheated thermal layer with a thickness of $\delta_{th,sat}$. The condensation starts when the height of the bubble is larger than $\delta_{th,sat}$. In pool boiling, the temperature distribution in the thermal layer is simplified to a linear one, that is

$$\delta_{th,sat} = \frac{T_{wall}-T_{sat}}{T_{wall}-T_{sub}} \cdot \delta_{th}. \quad (10)$$

In pool boiling, the total thermal layer thickness is considered to be at equilibrium conditions giving $\delta_{th} = (T_{wall} - T_{bulk})/(k_l \dot{q}_{wall})$ [21].

During the thermal diffusion controlled growth period the microlayer extends with the expansion of the bubble base and further supports the bubble growth. The newly formed part of the microlayer will be distributed based on the thickness at the outer border of the original microlayer.

2.2 Forces Acting on a Growing Bubble

For a bubble growing on a superheated surface a force balance analysis has been elaborated based on the work of Klausner et al. [9], Thorncroft et al. [13] and Chen et al. [14]. Considering the conservation of momentum in the direction tangential (subscript x) and the perpendicular (subscript y) to the heating surface, the forces acting on the bubble are given as

$$F_{total,y} = F_{growth,y} + F_{drag,y} + F_{cp,y} + F_{sl,y} + F_{b,y} + F_{surf,y}, \quad (11)$$

$$F_{total,x} = F_{growth,x} + F_{growth,b} + F_{drag,x} + F_{b,x} + F_{surf,x}. \quad (12)$$

F_{growth} is the bubble growth force, $F_{growth,b}$ is the added mass force due to the bubble growth in the bulk liquid field, F_{drag} is the quasi-steady drag force due to the viscous fluid flowing around the bubble, F_{cp} is the contact pressure due to the effect of the wall, F_b is the buoyancy force, F_{sl} is the lift force resulting from the asymmetrical flow distribution in the tangential direction of the wall, F_{surf} is the surface tension force due to the interfacial contact with the wall. In the conventional force balance model [9, 13, 14] for horizontal pool boiling the bubble departs or lifts off when the force becomes balanced in the perpendicular direction of the wall. In horizontal pool boiling, only the forces in the direction perpendicular to the wall will be considered.

2.2.1 Growth Force F_{growth}

In the study of Klausner et al. [9] a hemispherical bubble growing on a heating surface was considered. According to the Rayleigh equation, the pressure on a growing bubble in pool boiling is given as

$$\rho_l \left(r_b \ddot{r_b} + \frac{3\dot{r_b}^2}{2} \right) = p_l(r_b) \, . \tag{13}$$

By integrating the pressure difference distribution around the bubble $p_l(r_b)$ the force due to the expansion of bubble can be calculated. Due to the symmetric growth in the tangential direction in horizontal pool boiling the growth force in the tangential direction is 0 and the one in perpendicular direction can be expressed as

$$F_{growth,y} = -\rho_l \pi {r_w}^2 (r_b \ddot{r_b} + \frac{3\dot{r_b}^2}{2}). \tag{14}$$

Here, r_w is the bubble base radius which equals the bubble radius r_b when the bubble is hemispherical. Later, Chen et al. [14] extended this model to truncated spherical bubbles.

2.2.2 Drag Force F_{drag}

Due to the relative motion between bubble and liquid phase the quasi-steady drag force on the bubble in the perpendicular direction can be derived as

$$F_{drag,y} = 1/2 \rho_l {v_b}^2 \pi {r_b}^2 C_D, \tag{15}$$

where

$$v_b = \frac{dh_c}{dt}, \tag{16}$$

is the velocity of the bubble in the wall perpendicular direction and

$$h_c = \sqrt{r_b^2 - r_w^2} + r_b \tag{17}$$

is the height of bubble without bottleneck. C_D is the drag force coefficient, which depends on turbulence intensity, bubble Reynolds number and bubble shape. Due to the pre-assumption of a spherical bubble shape, C_D is simplified with the correlation proposed by Moore [23] and Clift et al. [24] as

$$C_D = \frac{16}{Re_b}(1 + 0.15{Re_b}^{0.5}). \quad (18)$$

Chen [14] considered this formula as not only valid for small Re_b, but also for $Re_b > 50$.

2.2.3 Contact Force F_{cp} and Buoyancy F_b

As a part of the bubble contacts the liquid and another part the heating surface, the effect of the total pressure acting on the outward surface of the bubble F_{tp} [14] can be expressed as

$$F_{tp} = F_b + F_{cp} + F_h, \quad (19)$$

where F_b, F_{cp}, F_h are the buoyancy force, contact pressure force and hydrodynamic force respectively.

For horizontal pool boiling the buoyancy is given as

$$F_{b,y} = (\rho_l - \rho_v)V_b g. \quad (20)$$

The contact pressure force, F_{cp}, is evaluated by the model of Thorncroft et al. [13], which only exists in the perpendicular direction of the heating surface and is given as

$$F_{cp} = \frac{1}{2}\pi {d_w}^2 \frac{\sigma}{r_c}. \quad (21)$$

Here, r_c is the radius of curvature at the points on the out border of bubble base (defined as $r_c = 5 \times r_b$ by Klausner et al. [9]) and σ is the surface tension. According to the study of Thorncroft et al. [13], the hydraulic dynamic force F_h includes the quasi-steady drag force, the shear lift force F_{sl} and the added mass force. In horizontal pool boiling, only the quasi-steady drag force is involved.

2.2.4 Surface Tension Force F_{surf}

At the interface between two materials, physical properties change rapidly over distances comparable to the molecular separation scale. Formally, surface tension is defined as the force per unit of length that acts orthogonally to an imaginary line drawn on the interface. For asymmetric bubbles contacting the heating wall the surface tension force in the tangential direction of the heating surface has been derived by Klausner et al. [9] as

$$F_{surf,y} = -2 * r_w * \sigma \frac{\pi}{\beta_{ad} - \beta_{re}}(\cos(\beta_{ad}) - \cos(\beta_{re})), \quad (22)$$

where r_w is the contact radius and β_{ad} and β_{re} are the advancing and receding angle of macrolayer. In the model the surface tension is dependent on the base diameter.

Zhao [21] investigated symmetric bubble growth in horizontal pool boiling where the advancing and receding angles are equal. They considered the formation of dryout during the bubble growth. In their model the surface tension only exists in the perpendicular direction and is dependent on dryout radius, which is given as

$$F_{surf,y} = 2 * \pi r_d \sigma \sin(\theta). \quad (23)$$

Here, θ is the contact angle of the microlayer to the wall. Because the microlayer evaporation depletion and dryout formation is also considered in the present model, the surface tension will depend on the dryout radius as well.

2.3 Contact Angle β and Bottleneck h_{bt}

2.3.1 Contact Angle

The contact angle plays an important role in the calculation of the forces on the bubble. However measurements and reliable models for the contact angle are rather scarce in previous studies. Klausner et al. [9] recommended $\beta_{ad} = \pi/4$ and $\beta_{re} = \pi/5$ from their measurements in R113 for flow boiling. As described and found by Mukherjee [25], the contact angle does vary during the ebullition cycle, as it is only dependent on the liquid and vapor properties and the material of the solid surface.

In this paper, we introduce a scheme to calculate the dynamic contact angle based on the analysis of forces. In horizontal pool boiling, when the bubble is in the inertia controlled period, the bubble is considered hemispherical when the contact angle is $\frac{\pi}{2}$. The surface tension, which keeps the bubble on the wall, is equal to 0 in this period because the dryout radius r_d is 0. However the fast expansion of the bubble prevents the bubble from departure. Further the dryout radius r_d increases when the sum of the negative forces which point toward the wall (mainly surface tension force) is much higher than the one of the positive forces (Figure 3). This negative total force will lead to a deformation of the bubble to reach the force balance in short time. In other words, the negative total force will drive the bubble to form a curvature and a contact angle to reduce the surface tension force in the negative direction until the forces on the bubble are balanced. The contact angle at which the force is again balanced is referred to as expected contact angle (β_s). From the force calculation this expected contact angle can be derived as

$$\beta_s = 2 * \text{asin}\left(\frac{F_{growth,y}+F_{drag,y}+F_{cp,y}+F_{sl,y}+F_{b,y}}{F_{surf}}\right). \quad (24)$$

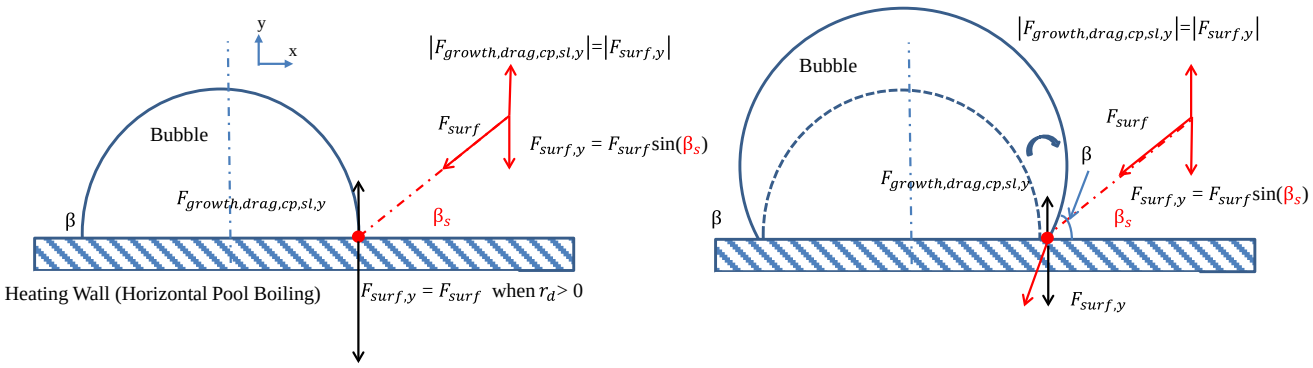

Figure 3: Bubble with dynamic contact angle β and expected contact angle β_s in pool boiling.

The constant 2 in Eq. (24) means that the contact angle β is two times of the microlayer contact angle θ, which is used to calculate the surface tension force in this work. β_s is continuously changing due to the change of forces during the bubble growth.

Further, β can be calculated with the base radius and the bubble radius as

$$\beta(t) = \arcsin\left(\frac{r_w(t)}{r_b(t)}\right). \tag{25}$$

It decreases from an initial value $\beta(0)=\frac{\pi}{2}$ towards the expected value β_s in some finite time interval. Due to the force balance and the increase of the positive forces in the wall perpendicular direction (i.e. buoyancy in horizontal pool boiling), β_s keeps increasing during bubble growth and consequently β will following this increase. If the force becomes positive during this time period, the bubble will start to depart and form a bottleneck.

2.3.2 Bottleneck

As stated by many researchers [4, 10-14] sphericity is considered as an important case dependent parameter, which needs recalibration to improve the accuracy of the model. In order to reduce the case dependency, the consideration of the bubble deformation during the bubble growth is required. In our model, the shape of bubble is first hemispherical in the inertia controlled growth period. Then it gradually changes from hemispherical to spherical during the thermal diffusion controlled period. Later it becomes a sphere plus a bottleneck according to the force balance. Finally it turns into a perfect sphere after lift-off.

In the bottleneck phase the bubble's main body starts departing but as the evaporation of microlayer still produces enough vapor the main body remains connected to the wall. The base diameter of the bubble starts to shrink when the evaporation of microlayer is less than required to form a new bottleneck. Unlike in the conventional force analysis model the bubble departure or lift-off criterion is that the bottleneck breaks up or the base diameter shrinks to 0. The bottleneck formation process is shown in the Figure 4.

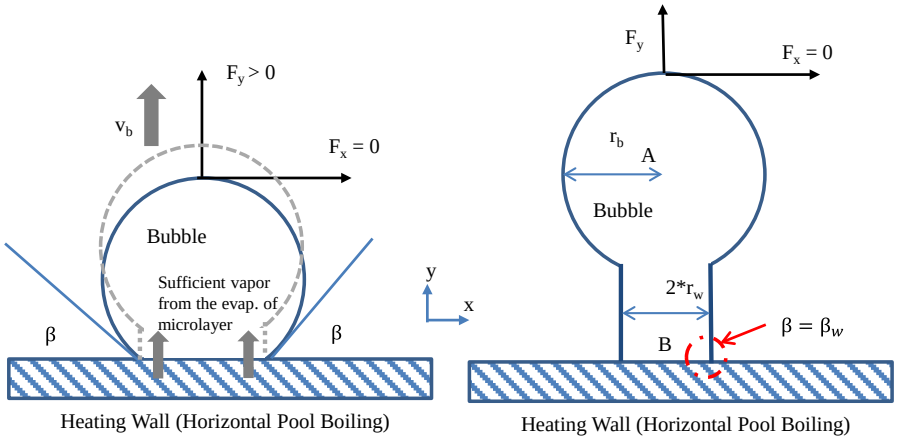

Figure 4: Formation of a bottleneck after the moment when force balance is reached and before bubble departure.

The contact angle of the bottleneck should depend on the wettability of the heater surface. Usually the contact angle of the bottleneck is considered as 90° which is larger than that during bubble growth. Therefore the total force becomes negative again during the bottleneck formation.

The base radius r_w will shrink when the $\dot{V}_{mig} < v_b \pi {r_w}^2$ due to volume conservation, that is

$$\frac{d(\pi {r_w}^2 h_{bt})}{dt} = \dot{V}_{mig} - v_b \pi {r_w}^2, \tag{26}$$

where h_{bt} is the height of bottleneck. The bottleneck height h_{bt} can be calculated from the bubble velocity and the time difference from the moment when the force becomes positive (t_{fp}) to the time point t according to

$$h_{bt} = v_b(t - t_{fp}). \tag{27}$$

When the microlayer is completely consumed or the pressure difference along the bottleneck reaches a limit, the bottleneck will break. From the Young-Laplace equation the pressure inside the bubble is given as

$$p = p_0 - \sigma\left(\frac{1}{R_1} + \frac{1}{R_2}\right). \tag{28}$$

Considering the bubble geometry in reality, the pressure at the bubble center point A and base point B (Figure 4) can be approximated as

$$p_A = p_0 - \sigma\left(\frac{1}{r_b} + \frac{1}{r_b}\right) \text{ and } p_B = p_0 - \sigma\left(\frac{1}{r_w} + \frac{1}{r_\infty}\right). \tag{29}$$

Further it can be considered that the pressure at point B must be balanced with that at point A following

$$p_B{}' = p_A + \frac{1}{2}\rho_g v_p^2 + \rho_g g h. \tag{30}$$

However due to the force acting on the bubble, $p_B{}'$ differs from p_B when p_B is strongly dependent on the base radius r_w. With the shrinking of r_w, p_B decreases. The difference $\Delta p_{B'B} = p_B{}' - p_B$ increases according to

$$\Delta p_{B'B} = \frac{1}{2}\rho_g v_p^2 + \rho_g g h + \sigma\left(\frac{1}{r_w} + \frac{1}{r_\infty} - \frac{2}{r_b}\right). \quad (31)$$

When $\Delta p_{B'B}$ is larger than the total force in perpendicular direction acting on the base radius, that is,

$$\Delta p_{B'B} \geq \frac{|F_{total,n}|}{A_{base}}, \quad (32)$$

the bottleneck will break up and the bubble will depart from the wall. Of course, if the base radius shrinks to 0 earlier, the bubble will also depart. The complete bubble growth and departure model for horizontal pool boiling is described in following scheme (Figure 4).

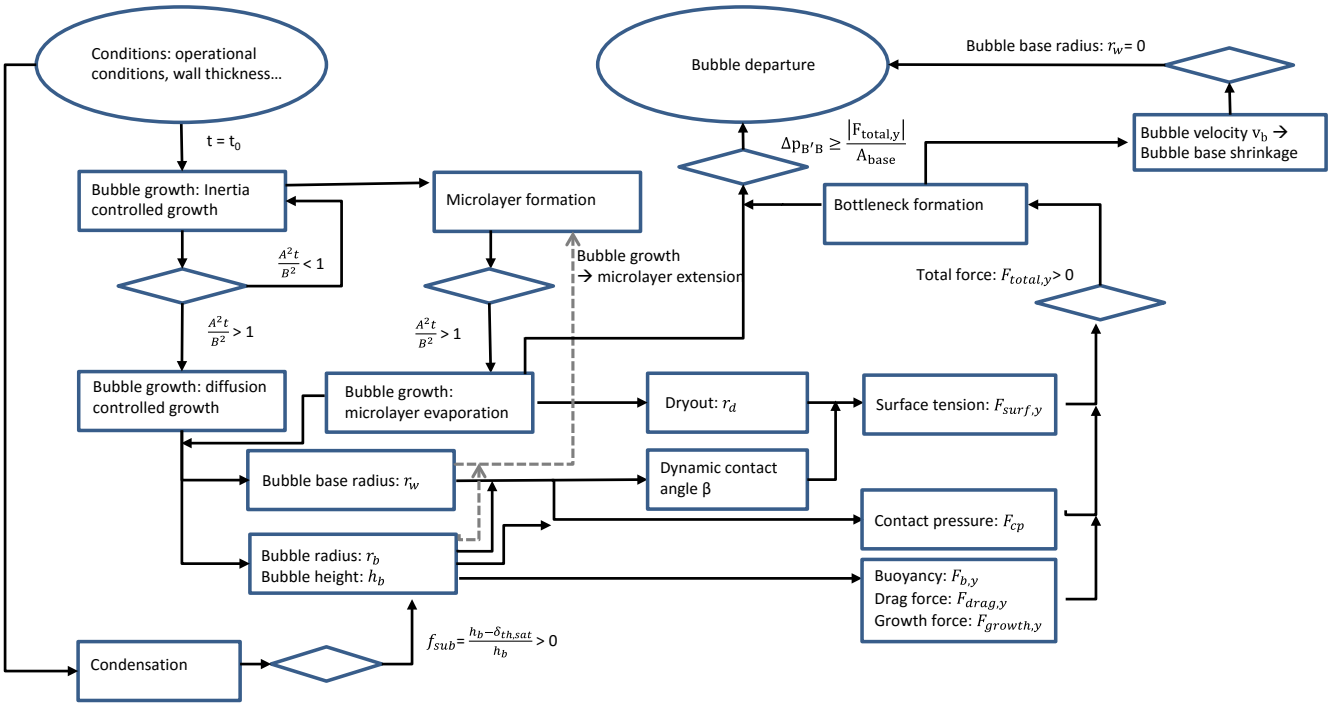

Figure 5: Scheme of the model including the sub-models for bubble growth and forces.

2.4 Base Diameter and Initial Microlayer Thickness

Also the base diameter is a key parameter which plays an important role in the force balance analysis. The deformation of the bubble causes the expansion of the base radius r_w with another rate than the growth of the bubble radius r_b. In Klausner's work, the authors considered $d_w = 2 * r_w$ as a constant of 0.09 mm. Later Thorncroft [13] adopted $d_w = 2r_b\sin(\beta)$ in order to improve the modelling accuracy. A constant ratio with bubble diameter $d_w = \frac{2r_b}{15}$ was used by Yun et al. [10]. In this work we prefer to consider the relationship between the expansion rate of base radius $\dot{r_w}$ and that of the bubble $\dot{r_b}$ instead of absolute values r_w and r_b (as in Thorncroft et al. [13]) in order to account for a smooth growth of bubble. Our approach is based on Thorncroft's work and so we express the expansion rate of r_w as

$$\dot{r_w} = \dot{r_b}\sin(\frac{\pi}{2} - \beta). \quad (33)$$

The initial microlayer thickness is defined as

$$\delta_{mi}^{0}(\mathrm{x}) = C_{mi}\sqrt{\nu_l \cdot t} = \sqrt{C\alpha_l \cdot \tau_g}, \qquad 0 \le t \le t_g \tag{34}$$

where the constants $C_{mi} = 0.8$ and $C = {C_{mi}}^2 Pr = 0.64 \cdot Pr$ were defined in Cooper's original paper [7], Pr is Prandtl number ν_l the kinematic viscosity of liquid, τ_g the microlayer formed time at position r in the bubble base and t_g the maximal inertia controlled growth time. Cooper et al. also pointed out that C has a range between $(0.09 \sim 1.0) \cdot Pr$ according to different experiments [7]. The microlayer thickness as a function of distance to the nucleation site is given as [21]

$$\delta_{mi}^{0}(x) = \frac{C\alpha_l \rho_g h_{fg} x}{2k_l \Delta T_{sat}}. \tag{35}$$

In earlier investigations [18] we found that C is a function of surface roughness and surface profile. Another more recent experimental correlation from Utaka et al. [26] for water boiling from a quartz glass surface (smooth) at atmospheric pressure is also considered, giving

$$\delta_{mi}^{0}(x) = 4.46e^{-3} * x. \tag{36}$$

However this correlation is valid only for water. From DNS calculations of Sato et al. [27] it was that C, as derived from Utaka's case, matches Duan's data for $\Delta T_{sat} = 9\,K$. In this work, we adapted Utaka's experimental data to Cooper's correlation resulting in $C = 0.0755 \cdot Pr$.

2.5 Heat Flux

2.5.1 Heat Flux Transfer from Wall to Liquid

The heat flux from the wall to liquid phase in the nucleate boiling process is divided into several terms: evaporation of microlayer $\dot{Q}_{e,mi}$, evaporation of macrolayer $\dot{Q}_{e,ma}$, heat transfer from wall to gas in the dryout $\dot{Q}_{dryout}$, quenching $\dot{Q}_q$ and single phase convection (wall to liquid) $\dot{Q}_{n,c}$, which are given as

$$\dot{Q}_{out} = \begin{cases} \dot{Q}_{e,mi} = \dot{m}_{mi} h_{fg} = \dfrac{k_l \Delta T_{sat}}{\delta_{mi}} & r_w > x > r_d \\ \dot{Q}_{e,ma} = \dot{m}_{ma} h_{fg} = \dfrac{k_l \Delta T_{sat}}{\delta_{ma}} & r_b > x > r_w \\ \dot{Q}_{dryout} = \dfrac{k_g \Delta T_{sat}}{\sqrt{\pi \alpha_g \tau_d}} & r_d > x \\ \dot{Q}_q = \dfrac{k_l \Delta T_{sat}}{\sqrt{\pi \alpha_l \tau_q}} & t > t_d \ (unif.T_{wall}) \ or \\ \dot{Q}_q = \dfrac{k_l \Delta T_{sat} \sqrt{\pi}}{2\sqrt{\alpha_l \tau_q}} & t > t_d \ (unif.\dot{Q}_{in}) \\ \dot{Q}_{n,c} = h_c (T_w - T_b) \quad flow\ boiling & x > r_b \ . \end{cases} \tag{37}$$

δ_{ma} is the distance between the interface to the wall in the wall perpendicular direction.

Quenching means the rewetting of the bulk liquid on the wall between the bubble departure and next activation. The formula is from Zhao's work [21].

2.5.2 Heat Transfer in the Wall

In the previous analyses the impact of wall thickness or wall material on the boiling heat transfer was usually not considered. However, as the wall can be a thermal buffer system with a high thermal conductivity it can impact the hot spot (dryout) underneath the bubble. In our model, the heat flux transferred in the wall tangential direction is considered and calculated. The heat flux in the wall tangential direction is given as

$$\dot{Q}_{t,w} = k_w \Delta T_{w,t} / \Delta L_w \ , \tag{38}$$

while the total heat flux through the wall is given as

$$\dot{Q}_{total} = \dot{Q}_{t,w} + \dot{Q}_{out} + \dot{Q}_{in}. \tag{39}$$

Considering energy conservation it follows, that

$$\frac{dT_w}{dt} = \dot{Q}_{total} / (c_{pw} \rho_w \delta_w). \tag{40}$$

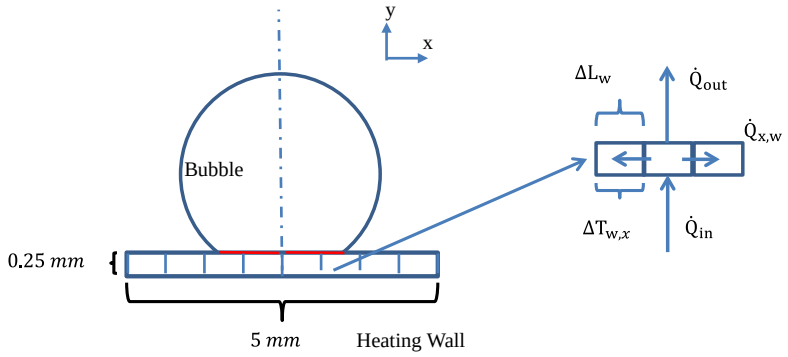

Figure 6 Scheme of the heat transfer along the wall underneath the bubble.

3. Results and Discussion

3.1 Experimental Database

In 2013, Duan et al. [19] used infrared thermometry and high speed video camera observation to investigate the bubble nucleation and heat transfer during pool boiling of water. Using a transparent indium-tin-oxid (ITO) heater (0.7 μm thick) on a Sapphire substrate (250 μm thick), it allowed the author to measure the temperature distribution, bubble contact diameter and other parameters from the bottom of the heater. Two cases were studied in Duan's experiment: case 1 is $T_{sup} = 9 \pm 2°C$, $\dot{Q} = 28.7 \pm 0.6\ kw/m^2$ under 1 bar and case 2 is $T_{sup} = 7.5 \pm 2°C$, $\dot{Q} = 36 \pm 0.7\ kw/m^2$ under 1 bar. Each experiment was repeated several times. The contact angle of water with the ITO wall surface (wettability) is $\frac{\pi}{2}$ and was obtained in experiments with the same facility performed by Gerardi et al. in 2009 [28].

Recently, Sato and Niceno [20] developed a new direct numerical simulation model based on Color Functions. In their model they simulated the dry spot underneath the bubble and determined the bubble growth rate, shape change and the temperature distribution on the heater surface, which were in good agreement with experimental data. The disadvantage of a DNS simulation is that the simulation domain is strictly limited to the millimeter to centimeter range for reasons of limited computational power. Hence for large scale simulations (~ dm or m) simplified sub-models, as the one presented here are still required.

The simulation results from our sublayer model were compared with Duan's experiments and further with Sato's DNS. Moreover, the temperature distribution around the cavity and frequency have been analysed to compare modelling and experiments for Duan's case too. In the calculation, the bubble growth model is considered as a one dimension model which requires a time discretization. The microlayer and heat transfer on the wall is considered as a two dimension model which requires a tangential direction spatial discretization. The size of the wall in the model taken from Duan's case is 0.25 mm x 5 mm.

3.2 Discretization Dependency Study

The sub-model requires a time discretization for bubble dynamics and space discretization for the microlayer and the heat transfer inside the wall tangential direction. Both time and space are all discretized using a central differences scheme. The CFL number is controlled to be less than 1. Nine cases with temporal step length from 1 μs to 30 μs and spatial step length from 10 μm to 50 μm were tested. The simulation case is pool boiling at 1 bar with water. The results for bubble lift-off diameter for different discretization sizes are shown in the following.

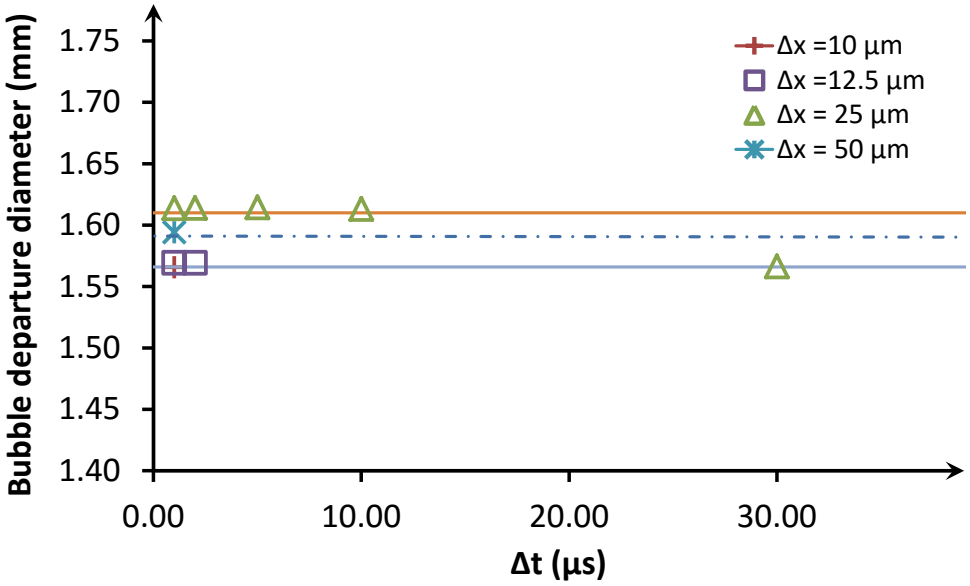

Figure 7: Calculated bubble lift-off diameter for different space and time discretization

The deviation from the average value for all 9 cases is less than +1.47% and -1.60%. When the spatial step length is less than 50 µm and temporal step length is less than 30 µs the model converges well.

3.3 Comparison of the Model with Experiment, DNS in Pool Boiling Case

As mentioned, the geometry change is tracked in our model. Figure 8 shows the geometry of the bubble from activation to lift-off (departure) from the wall. The first row of the images is taken from Duan et al. [19] (experiment). The second row is the DNS calculation at the same conditions (Sato et al. [27]). The third row is from our model. With our model, the bubble shape is hemispherical at activation t = 0 ms, then changes from hemispherical to spherical during growth until t = 6.9 ms, and further changes to a truncated sphere plus bottleneck as a balloon at t = 12 ms (experiment at t ≈ 13.2 ms). Of course the experiment and DNS calculation do not result in perfect hemispheres or spheres, but qualitatively the bubble shape agrees still well among the three cases. Overall, our model reproduces the bubble dynamic geometry during the bubble growth. As a qualitative comparison is not enough for the validation, a further quantitative comparison is given in Figure 9.

	Time [ms]	0 (Bubble nucleation)	0.7	2.8	6.9	13.2
Experiment (Duan 2013)	**HSV images**	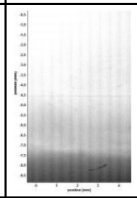	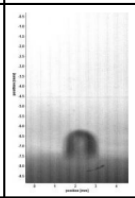	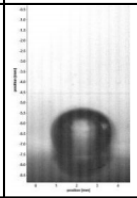	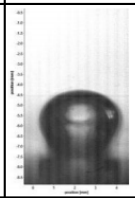	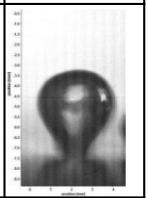
DNS calculation (Sato 2015)		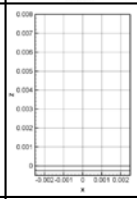	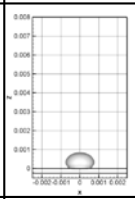	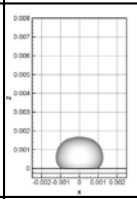	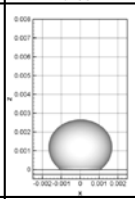	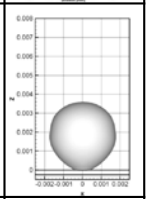
Present model				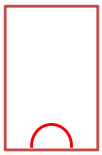	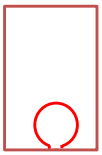	**~ 12 ms** 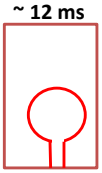

Figure 8: Geometry of the bubble at different growth period from experiments of Duan et al. [19], DNS calculations from Sato [27] and calculation with our model under the same conditions.

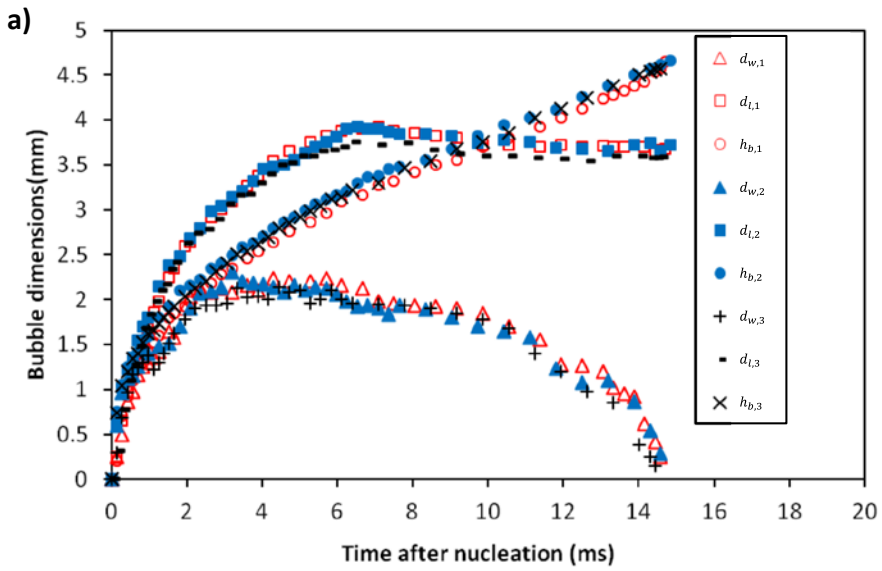
a)
Bubble dimensions(mm)
Time after nucleation (ms)
$d_{w,1}$
$d_{l,1}$
$h_{b,1}$
$d_{w,2}$
$d_{l,2}$
$h_{b,2}$
$d_{w,3}$
$d_{l,3}$
$h_{b,3}$

419

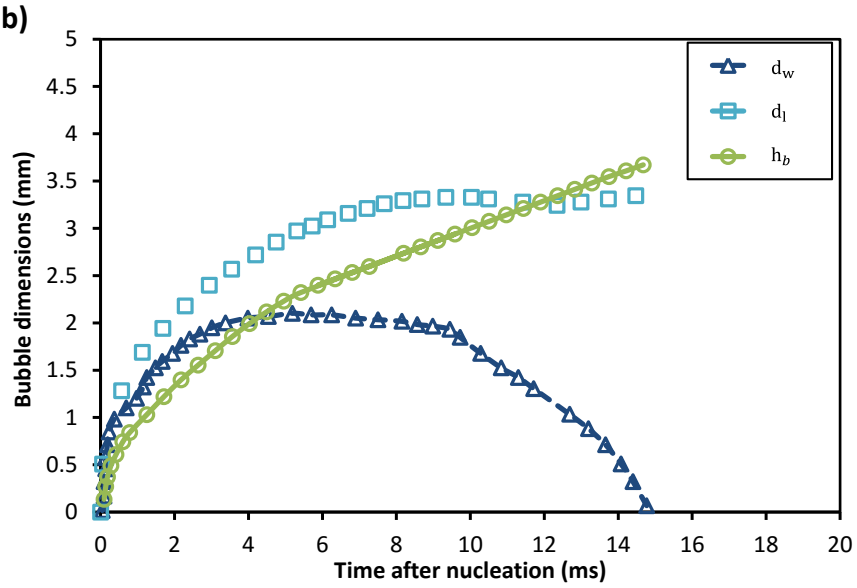
b)
Bubble dimensions (mm)
Time after nucleation (ms)
d_w
d_l
h_b

420

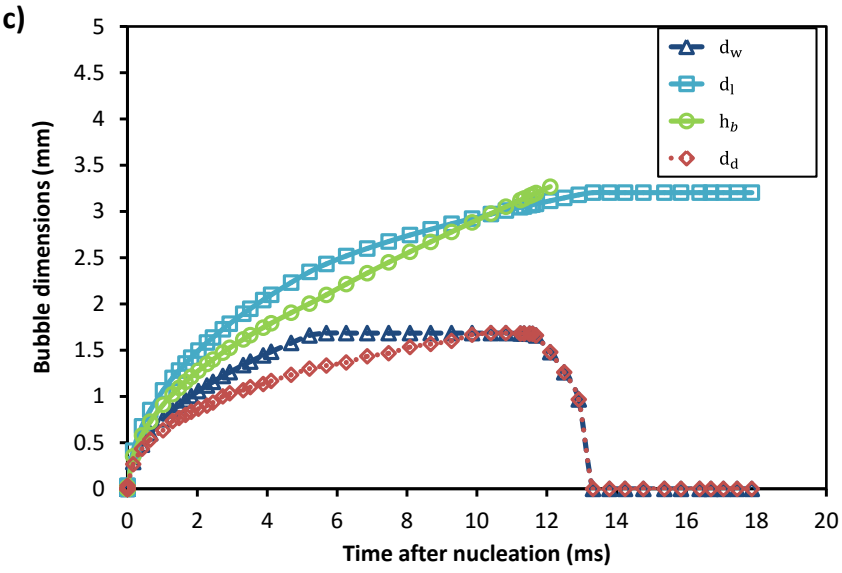
c)
Bubble dimensions (mm)
Time after nucleation (ms)
d_w
d_l
h_b
d_d

421

Figure 9: Bubble dynamics from a) three bubbles under same condition in Duan et al.'s experiments [19], b) Sato et al.'s DNS calculations [27] and c) our model under the same conditions. d_w is the base diameter, d_l is the lateral diameter, h_b is the bubble height and d_d is the dryout diameter.

The bubble departure time in the experiment and DNS calculation is around 15 ms, while that in the present calculation is around 13.3 ms. The maximal lateral bubble diameter in the experiment is around 3.9 mm and for DNS around 3.5 mm. The lateral diameter at the departure moment is around 3.6 mm and 3.4 mm in experiment and DNS respectively. The none-perfectly spherical geometry of the bubble in the experiment and DNS causes the obtained lateral diameter of bubble to differ from the equivalent one. The equivalent bubble departure diameter is 3.8 ± 0.08 mm in the experiment. Due to the perfect hemispherical, spherical and sphere plus bottleneck setup in our model, the maximal lateral diameter and the diameter at departure are 3.2 mm in all cases. The difference between the departure diameter predicted by our model, the one of the experiment and the one of the DNS is only 16% and 6%.

As mentioned above, our model considers the microlayer which contributes to bubble growth and the formation of dryout area underneath the bubble. The dryout area can be measured or observed from the temperature distribution on the wall. Duan et al. measured the temperature distribution under the bubble on the wall with an IR camera through the ITO heater and Sapphire substrate (Figure 10).

	Time [ms]	0 (Bubble nucleation)	0.7	2.8	6.9	13.2
Experiment (Duan 2013)	IR images	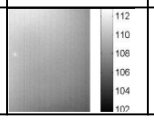	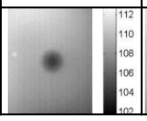	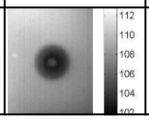	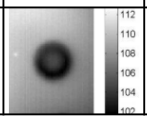	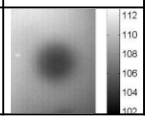

Figure 10: Temperature distribution underneath bubble on the wall measured with IR camera by Duan et al. [19].

Duan et al. measured the temperature distribution in a radius of 2.5 mm from bubble activation (t = 0) to complete bubble departure from the wall (t = 15 ms) until the bubble was far away from the wall (t = 117.44 ms) (Figure 11a). When the microlayer underneath the bubble is completely evaporated, the dryout area will form, which has very low heat transfer coefficient because the gas directly contacts the wall and there is no evaporative heat transfer any more. The temperature in the dryout area then accordingly increases. This high temperature was observed by Duan from t = 2.5 ms until t = 8.75 ms. The dryout area is rewetted again after bubble departure at t = 15 ms. Then the wall is also again reheated until the nucleate site gets back to activation temperature, which is 109°C in this case. The position (r) of the lowest temperature values along the surface indicates the radius of base underneath the bubble from t = 2.5 ms to t = 8.75 ms.

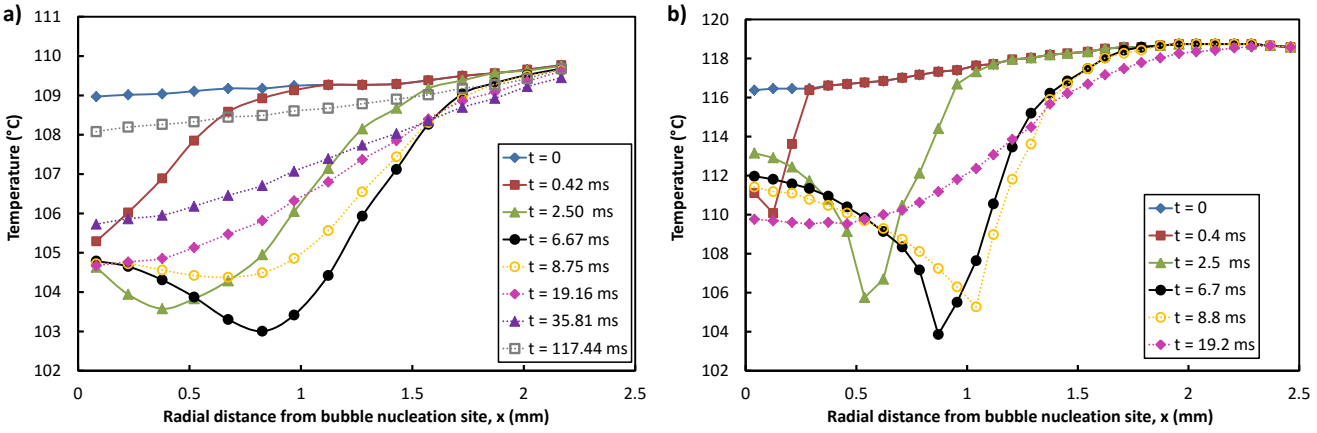

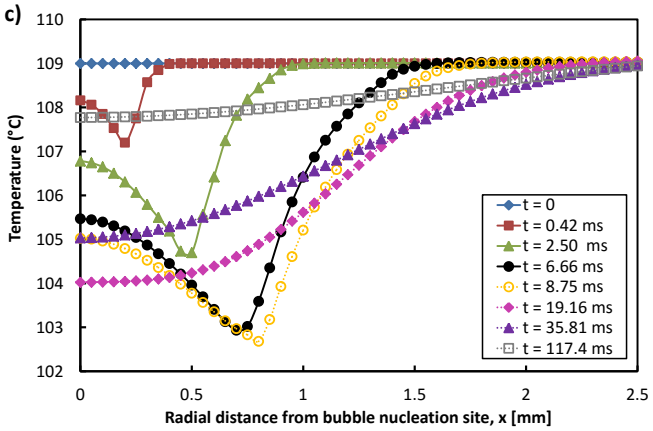

Figure 11: Temperature distribution on the wall at different times during the bubble growth: a) experiment from Duan et al. [19], b) DNS from Sato et al. [27] c) our model.

As shown in Figure 11 b), Sato et al. also analyzed the temperature distribution around the cavity. However, he found the dryout arises after a very short time (t = 0.4 ms) following activation. The temperature distribution between t = 0.4 and t = 8.8 ms has a much sharper turning point at the edge of the bubble base than that in the experiment. The reason may be that the sapphire substrate blurs the resolution of temperature profile, while the DNS calculation and our model calculation give the temperature on the wall surface directly. Nonetheless, our model still has a good agreement with experimental results and DNS in the temperature distribution profile.

Table 2: Comparison between model prediction and experimental data of Duan [19]

	Exp (case 1)	Model	Error ($_{Abs(Model-Exp)/Exp}$)
Bubble growth time	15 ms	13 ms	13%
Waiting time	200 ms	221 ms	10%
	Exp (case 2)	Model	
Bubble growth time	16 ms	16 ms	0
Waiting time	52 ms	83 ms	59%

The comparison between the experimentally measured bubble growth time and waiting time and modelled value is shown in Table 2. From the experiment it is found that for case 1 there is a bubble growth time of 15 ms and a waiting time of 200 ms. While it is 16 ms and 52 ms in case 2. The calculated bubble growth time is 13 ms and waiting time is 221 ms in case 1. The growth time is 16 ms and waiting time is 83 ms in case 2.

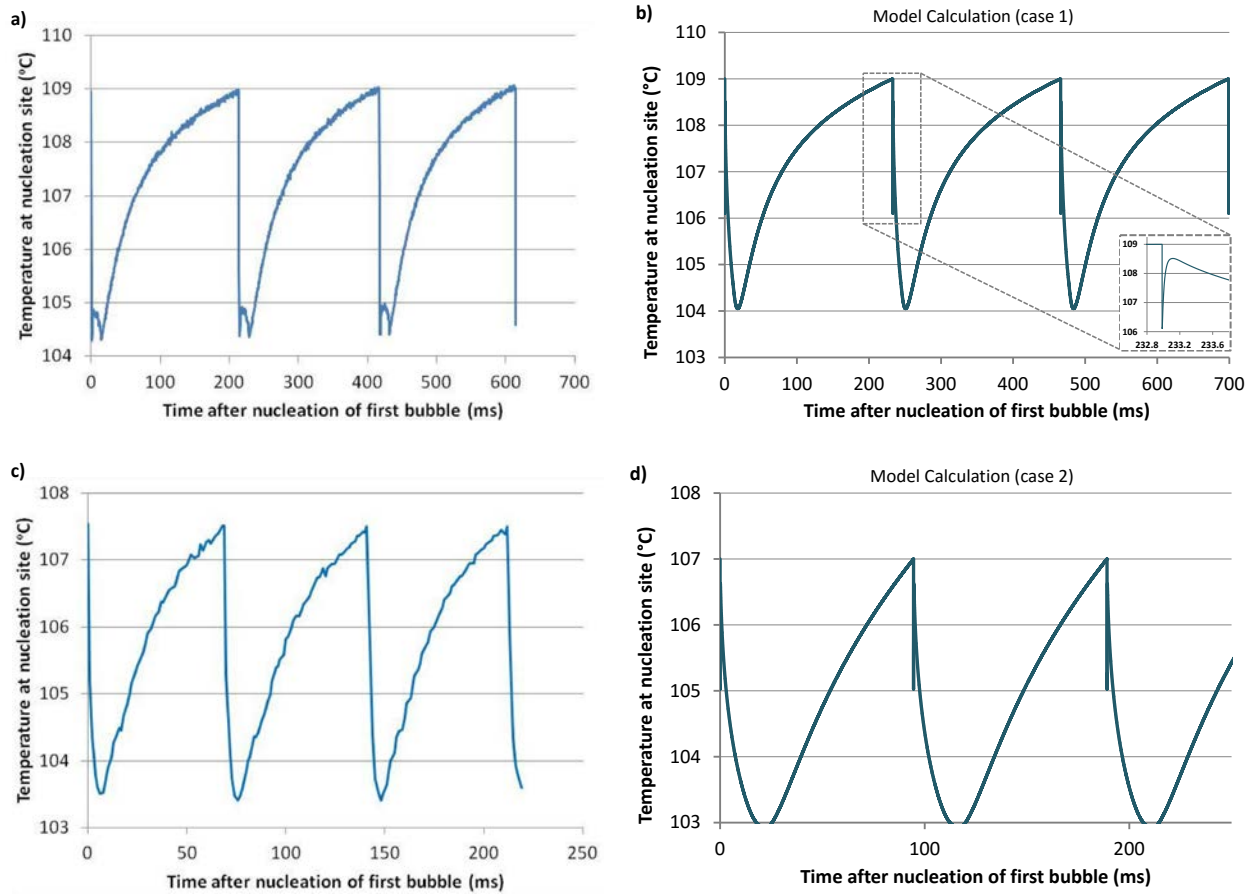

Figure 12: Temperature history of the nucleation site a) Duan's experiment case 1; b) Model calculation under conditions of case 1; c) Duan's experiment in case 2; d) Model calculation under conditions of case 2.

The fast and abrupt decrease and increase of the temperature at the nucleation site (insert in Figure 12 b) is related to the temperature change at x = 0 in Figure 11. The difference between our model calculation and experiment is in the range of ~ 13% ((Model-Exp)/Exp*100%) for growth time, ~10% for waiting time in case 1; and ~ 0% for growth time, ~59% for waiting time in case 2.

3.4 Comparison of Different Approaches for Contact Angle and Base Diameter

In order to analyse the efficacy of the consideration of dynamic contact angle and base expansion in our model, we analysed five different modelling scenarios:

1. A constant contact angle and a constant base diameter [9] which expands in the inertial growth period [21];
2. A dynamic contact angle and constant base diameter [19] which expands in the inertial growth period [21];
3. A constant contact angle and a base diameter expansion following Thorncroft et al. [13];
4. A dynamic contact angle and a base diameter expansion following Yun's work [10] and
5. A dynamic contact angle and a base diameter expansion following our model.

The five scenarios and their main parameters are further summarized in the Table 3. In the constant base diameter cases, the maximal inertia controlled bubble radius ($r_{m,g}$) is set to 0.09 mm. Having reached this value the bubble geometry changes from hemispherical to truncated spherical.

Table 3: Overview of the model variations used to clarify the different approaches for base diameter expansion and contact angle

Scenario	1	2	3	4	5
Contact angle	$\frac{\pi}{4}$ Klausner et al. [9]	Dynamic contact angle	$\frac{\pi}{4}$ Klausner et al.	Dynamic contact angle	Dynamic contact angle
Base Diameter Expansion	$d_w = 0.09$ mm Klausner et al. [19]	$d_w = 0.09$ mm Klausner et al. [9]	$d_w = 2r_b\sin(\beta)$ Thorncroft et al. [13]	$d_w = 2r_b/15$ Yun et al. [10]	$\dot{r_w} = \dot{r_b}\sin(\frac{\pi}{2} - \beta)$
Bottleneck	No	Yes	No	Yes	Yes

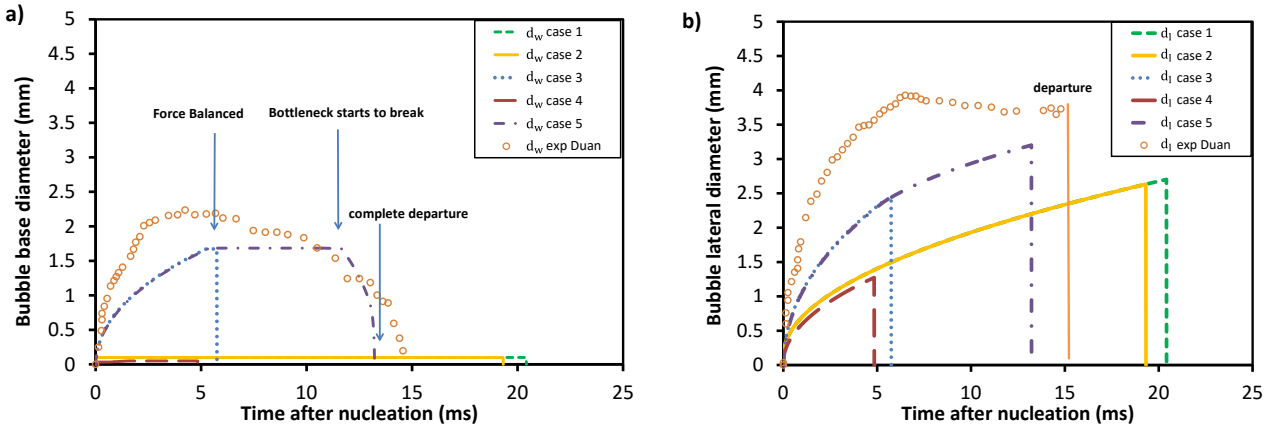

Figure 13: Base (d_w) and lateral diameter (d_l) calculated with different bubble base expansion rules and constant or dynamic contact angle

From the comparison of the conventional setups from the former investigations, it can be found that our model (case 5) has a better agreement to the Duan's experiment (Figure 13) among the investigated mechanistic models. However, the present model still underestimated the base diameter and bubble growth speed. This deviation may be caused by the regular spherical setup of bubble's main body in the model while the bubble is not a perfect spherical in the experiment and DNS.

In case 1 and case 2 the microlayer contributes much less to the bubble growth than other three cases, because the base diameter is only 0.09 mm, which is much lower than that of Thorncroft et al. [13] and our model. Even the departure time is longer but the bubble size is much smaller than for cases 3 and 5. Compared to cases 1 and 2, the base diameter of case 4 is even smaller which leads to the shorter departure time and smaller bubble departure diameter.

From the departure criterion in Klausner's work [9], the bubble will depart when the forces are balanced in the wall perpendicular direction for horizontal pool boiling, as shown in case 3. Due to the negligence of the geometry change the bubble departs much earlier than in case 5. The bubble lateral diameter in case 3 is only 75% of the one in case 5 (Figure 13).

3.5 Contribution of Microlayer, Macrolayer and Condensation to the Bubble Growth

The contribution of the microlayer to the bubble growth will be discussed here.

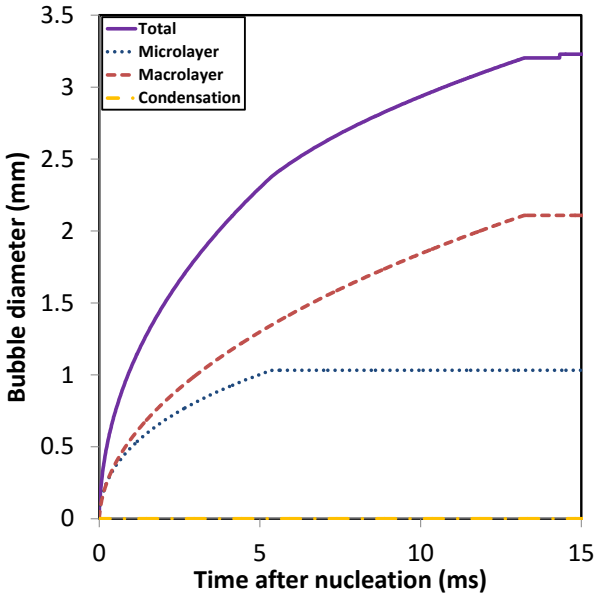

Figure 14: Contribution of the microlayer, macrolayer and condensation to the bubble growth (bubble diameter) during the bubble growing transient in saturate pool boiling under conditions of Duan's case 1.

When the pool boiling is saturated there is no condensation anymore. In the inertia controlled period, the microlayer evaporation is then the only contribution to the bubble growth. Later, during the thermal controlled growth period, the macrolayer contributes more and more from 0 to 56% to the bubble diameter at t = 5.4 ms and gets the dominant share to growth contribution especially after t = 5.4 ms when the microlayer is completely dried out (Figure 14a). When the bubble departs at t = 13.3 ms, the macrolayer contributes to 68% of the total bubble diameter. This contribution of the microlayer is around 32%, which is similar to the value of 30% from experimental results of Chu [29] but smaller than the 55% calculated by DNS in Sato's work [27]. As the initial microlayer thickness (Eq. (35)) is inversely proportional to the wall superheat, the total contribution from the microlayer becomes less when the wall superheat is higher. This agrees qualitatively with the experimental data of Jung et al. [30], where contribution is 17% for 20 K superheat.

With a multitude of calculations for different experiments from Duan et al. [19], Klausner et al. [9], Situ et al. [11] and Sugure et al. [12], in the proposed model, the microlayer contact angle θ in Eq. (23) is suggested as half of contact angle of the macrolayer β (Figure 2) when the dryout radius r_d is smaller than the contact based radius r_w. When r_d increases to r_w, θ will be equal to β. The r_∞ applied in Eq. (31) is suggested to be equal to r_w.

4. Conclusions

A mechanistic model of bubble behavior during boiling has been developed for both pool boiling and flow boiling. The application of the model for the horizontal pool boiling case was introduced in this work. The model includes several well developed conventional theories and sub-models with or without modification and some new concepts. It covers the whole bubble life cycle including inertia controlled, thermal diffusion controlled and departure periods. The microlayer, which forms during the inertia controlled growth period and the bubble base expansion, contributes to the bubble growth in this model. The force balance equations based on Klausner et al., Throncroft et al. and Chen et al. were applied to determine the departure of the bubble. The consideration of dynamic contact angle and dynamic bubble base expansion further allows the model to track microlayer formation, evaporation

and depletion process during bubble growth. It also allows tracking the bubble geometry change from hemisphere to truncated sphere and further to sphere plus bottleneck continuously.

The calculated bubble dynamics such as growth dimensions at different time, departure diameter, base diameter, dryout diameter, growth and waiting time are in good agreement with the available experimental data. It shows the high accuracy of the integral model of bubble growth in our approach. Moreover, the good agreement of the calculated temperature distribution along the heating wall with the experimentally measured data shows the correctness of our microlayer model. The microlayer model is strongly impacted by the dynamic contact angle and base expansion. The good agreement also verifies these two ideas. Later, these ideas described in this work will be applied to calculate the bubble dynamics in the flow boiling covering different conditions.

From our model it is found that only the force balance is not enough to predict the bubble departure in the horizontal pool boiling. The delay of the bubble departure due to the bubble deformation during the bubble growth (bottleneck) after force balance should be taken into account as well.

Acknowledgments

This work was funded by the German Federal Ministry of Economic Affairs and Energy (BMWi) under grant number 1501473C on the basis of a decision by the German Bundestag.

Nomenclature

A_b	bubble surface area
A_{ma}	area of macrolayer
C	constant from Cooper
c_D	friction drag coefficient
c_{pl}	specific heat capacity of liquid
c_{pw}	specific heat capacity of wall
d_l	bubble lateral diameter
d_w	bubble base diameter
$F_{b,v,y}$	buoyancy in wall perpendicular direction
$F_{cp,y}$	contact pressure force in wall perpendicular direction
$F_{drag,y}$	drag force in wall perpendicular direction
$F_{growth,b}$	growth force in bulk
$F_{growth,y}$	growth force in wall perpendicular direction
$F_{sl,y}$	sliding lift force in wall perpendicular direction (flow boiling)
$F_{surf,y}$	surface tension in wall perpendicular direction
$F_{total,x}$	total force in wall tangential direction
$F_{b,x}$	buoyancy in wall tangential direction

578	$F_{drag,x}$	drag force in wall tangential direction
579	$F_{growth,x}$	growth force in wall tangential direction
580	$F_{surf,x}$	surface tension in wall tangential direction
581	$F_{sl,x}$	sliding lift force in wall tangential direction
582	f_{sub}	the portion of the bubble surface in contact with sub cooled liquid
583	h_b	height of bubble top to the wall
584	h_{bt}	height of bottleneck
585	h_c	height of bubble center to the wall
586	h_{fg}	latent heat
587	k_l	thermal conductivity of fluid in liquid phase
588	k_g	thermal conductivity of fluid in gas phase
589	k_w	thermal conductivity of wall
590	$\dot{m}_{ma}$	mass flow of evaporated liquid in macrolayer
591	$\dot{m}_{mi}$	mass flow of evaporated liquid in microlayer
592	P_l	pressure difference on the bubble interface
593	P_r	Prandtl number
594	$\dot{Q}_{in}$	heat flux entering into wall
595	$\dot{Q}_{out}$	total heat flux from wall to fluid
596	$\dot{Q}_{e,mi}$	heat flux due to evaporation of microlayer
597	$\dot{Q}_{e,ma}$	heat flux due to evaporation of macrolayer
598	$\dot{Q}_{dryout}$	heat flux due to dryout
599	$\dot{Q}_q$	heat flux due to quenching
600	$\dot{Q}_g$	heat flux due to gas film (hotspot)
601	$\dot{Q}_{n,c}$	heat flux due to natural convection
602	$\dot{Q}_{total,w}$	total heat flux of a wall segment
603	$\dot{Q}_{n,w}$	conduction heat flux between neighboring wall segments
604	r	r coordinate/position
605	r_b	bubble radius
606	r_d	bubble dryout radius
607	$r_{m,g}$	maximum radius in initial growth regime
608	r_w	bubble contact radius (base radius)
609	Re_b	Reynold's number of bubble

610	T_b	bulk temperature
611	T_w	wall temperature
612	T_∞	temperature in the bubble in the inertia controlled growth regime
613	T_{sat}	saturation temperature
614	T_{sub}	subcooling temperature
615	t	time
616	t_d	time of departure
617	t_g	maximal inertia controlled growth time
618	τ_g	maximal inertia controlled growth time at different r position
619	τ_d	time counted from dryout starting
620	τ_q	time counted from quenching starting
621	v_b	bubble velocity in wall perpendicular direction
622	V_b	volume of bubble
623	$\dot{V}_{mi,g}$	total volume of formed gas
624	$\dot{V}_{mi,l}$	total volume of evaporated liquid
625	ΔL_w	distance between two neighboring wall segments
626	ΔT_w	temperature difference between two neighboring wall segments
627	ΔT_{sat}	super heating
628	ΔT_{sub}	subcooling
629	α_l	thermal diffusivity of fluid in liquid phase
630	α_g	thermal diffusivity of gas in liquid phase
631	β	contact angle of macrolayer in horizontal pool boiling
632	β_{ad}	advancing contact angle of macrolayer in flow boiling
633	β_{re}	receding contact angle of macrolayer in flow boiling
634	β_s	expected contact angle
635	θ	contact angle of microlayer
636	θ_w	wall orientation angle
637	σ	surface tension
638	ρ_g	density of vapor
639	ρ_l	density of vapor
640	ρ_w	density of wall
641	δ_{mi}^0	initial microlayer thickness at time t_g
642	δ_{mi}	microlayer thickness

δ_w	wall thickness
δ_{th}	thickness of thermal layer
Subscript:	
dryout	at dryout area
e	evaporation
g	gas phase
l	liquid phase
mi	microlayer
ma	macrolayer
n,c	natural convection
w	wall
y	wall perpendicular direction
x	wall tangential direction

References

[1] H.K. Forster, N. Zuber, Growth of a vapour bubble in a superheated liquid, J. Appl. Phys. 25, (1954) 474–478.

[2] M.S. Plesset, S.A. Zwick, The growth of vapour bubbles in superheated liquids, J. Appl. Phys. 25 (1954) 493–500.

[3] N. Zuber, The dynamics of vapor bubbles in nonuniform temperature fields, Int. J. Heat Mass Transfer 2 (1961) 83–98

[4] B.B. Mikic, W.M. Rohsenow, P. Griffith, On bubble growth rates, Int. J. Heat Mass Transfer 13, (1970) 657–666.

[5] A. Prosperetti, M.S. Plesset, Vapour-bubble growth in a superheated liquid, Journal of Fluid Mechanics, (1978) 85, 349

[6] D.A. Labuntsov, State of the art of the nucleate boiling mechanism of liquids. Heat ransfer and Physical Hydrodynamics, Moskva, Nauka, in Russian (1974) 98–115.

[7] M.G. Cooper, A.J.P. Lloyd, The microlayer in nucleate pool boiling, Int. J. Heat Mass Transfer 12 (1969) 895–913.

[8] S.J.D. van Stralen, M.S. Sohal, R. Cole, W.M. Sluyter, Bubble growth rates in pure and binary systems: combined effect of relaxation and evaporation microlayers, Int. J. Heat Mass Transfer 18 (1975) 453–467

[9] J.F. Klausner, R. Mei, D.M. Bernhard, L.Z. Zheng, Vapor bubble departure in forced convection boiling, Int. J. Heat Mass Transfer 36 (1993) 651–662

[10] B. J. Yun, A. Splawski, S. Lo, , C. Song, Prediction of a subcooled boiling flow with advanced two-phase flow models, *Nuclear Engineering and Design, 253* (2012) 351-359.

[11] R. Situ, T. Hibiki, M. Ishii, M. Mori, Bubble lift-off size in forced convective subcooled boiling flow, Int. J. Heat Mass Transfer 48 (2005) 5536–5548.

[12] R.M. Sugrue, The effects of orientation angle, subcooling, heat flux, mass flux, and pressure on bubble growth and detachment in subcooled flow boiling, Master Thesis in Nuclear Science and Engineering, Massachusetts Institute of Technology, Cambridge, MA, 2012

[13] G.E. Thorncroft,, J.F.Klausner, R. Mei, Bubble forces and detachment models. Multiphase Science and Technology 13, (2001) 35–76.

[14] D.Q. Chen, L.M. Pan, S. Ren, Prediction of bubble detachment diameter in flow boiling based on force analysis, Nuclear Engineering and Design 243 (2012) 263–271

[15] M. Colombo, M. Fairweather, Prediction of bubble departure in forced convection boiling: A mechanistic model, Int. J. Heat Mass Transfer 85 (2015) 135–146.

[16] S. Raj, M. Pathak, M. K: Khan, An analytical model for predicting growth rate and departure diameter of a bubble in subcooled flow boiling, Int. J. Heat Mass Transfer 109 (2017) 470-481.

[17] T. Mozzocco, W. Ambrosini, R. Kommajosyula, E. Baglietto, A reassessed model for mechanistic predition of bubble departure and lift off diameter, Int. J. Heat Mass Transfer 117 (2018), 119-124

[18] D Sarker, R. Franz, W. Ding, U. Hampel. Single bubble dynamics during subcooled nucleate boiling on a vertical heater surface: An experimental analysis of the effects of surface characteristics. International Journal of Heat and Mass Transfer 109:907-921, (2017) DOI: 10.1016/j.ijheatmasstransfer.2017.02.017

[19] X. Duan, B. Phillips, T. McKrell, and J. Buongiorno. “Synchronized High-Speed Video, Infrared Thermometry, and Particle Image Velocimetry Data for Validation of InterfaceTracking Simulations of Nucleate Boiling Phenomena.” Experimental Heat Transfer 26, no. 2 3 (March 2013): 169-197

[20] Y. Sato, B. Niceno, A sharp-interface phase change model for a mass-conservative interface tracking method, *J. Comput. Phys.,* 249, (2013) 127-161.

[21] Y.H. Zhao, and T. Tsuruta, Prediction of bubble behavior insubcooled pool boiling based on microlayer model, JSME Int. J. Vol. 45, No. 2, (2002) 346-354

[22] W.E. Ranz, W.R. Marshall, Evaporation from drops, Chem. Eng. Prog. 48 (1952) 141–146.

[23] D.W. Moore, The boundary layer on a spherical gas bubble. Journal of Fluid Mechanics 16, (1963) 161 – 176

[24] R. Clift, J.R. Grace, M.E. Weber, Bubble Drops and Particles. Academic Press, New York (1987).

[25] A. Mukherjee, S.G. Kandlikar, Numerical study of single bubbles with dynamic contact angle during nucleate pool boiling, International Journal of Heat and Mass Transfer 50 (2007) 127 – 138

[26] Y. Utaka, Y. Kashiwabara, M. Ozaki, Microlayer structure in nucleate boiling of water and ethanol at atmospheric pressure, Int. J. Heat and Mass Transfer 57 (2013) 222–230

[27] Y. Sato and B. Niceno, A delpletable micro-layer model for nucleate pool boiling, J. Computational physics 300 (2015) 20-52

[28] J.C. Chen, “Correlation for boiling heat transfer to saturated fluids in convective flow”, Ind. Eng. Chem. Res. 5 pp. 322–329, (1966).

[28] C. Gerardi, J. Buongiorno, L. Hu, T. McKrell, Study of bubble growth in water pool boiling through synchronized, infrared thermometry and high-speed video, Int. J. Heat Mass Transfer 53 (2010) 4185–4192.

[29] I.C. Chu, Application of Visualization Techniques to the Boiling Structures of Subcooled Boiling Flow and Critical Heat Flux (Ph. D dissertation), Korea Advanced Institute of Science and Technology, 2011

[30] S. Jung, H. Kim, An experimental method to simultaneously measure the dynamics and heat transfer associated with a single bubble during nucleate boiling on a horizontal surface, International Journal of Heat and Mass Transfer 73 (2014) 365-375